

THE TERRASAR-X PRECISE ORBIT CONTROL – CONCEPT AND FLIGHT RESULTS

Ralph Kahle⁽¹⁾ and Simone D’Amico⁽²⁾

⁽¹⁾ German Space Operation Center (DLR/GSOC), 82234 Wessling, Germany, Phone: +49 8153 282451, ralph.kahle@dlr.de

⁽²⁾ Stanford University, Department of Aeronautics & Astronautics, W.F. Durand Building, 496 Lomita Mall, Stanford, CA 94305-4035, USA, Phone: (650) 497-4682, damicos@stanford.edu

Abstract: TerraSAR-X is an advanced synthetic aperture radar satellite system operated in a 505 km altitude sun-synchronous repeat orbit. A tight orbit control requirement, driven by interferometric applications, is formulated as a 250 m radius “tube” defined about an Earth-fixed reference orbit. In this paper we review the orbit control requirements and constraints and discuss the implemented guidance and control concept. Since the launch in 2007 more than six years of in-flight experience have been gained, including almost 500 orbit control maneuvers. The presented flight results proof that both the implemented reference orbit and the orbit control concept work remarkably well, and that the tight control requirement is fully met.

Keywords: TerraSAR-X, Orbit Control, Flight Dynamics Operations

1. Introduction

TerraSAR-X (TSX) is Germany’s first Earth observation synthetic aperture radar (SAR) satellite mission that carries an advanced high-frequency multimode SAR X-band sensor [1]. The spacecraft was launched on a Russian DNEPR rocket on June 15, 2007 from Baikonur, Kazakhstan, and since then has been operated in a 505 km sun-synchronous dusk-dawn orbit with an 11-day repeat cycle. TSX supplies high quality radar data for scientific Earth observation as well as for commercial applications. The broad spectrum of applications includes hydrology, geology, climatology, oceanography, environmental and disaster monitoring, as well as cartography and interferometry.

Especially SAR interferometry drives the accuracy requirements for flight dynamics operations with respect to guidance, navigation and control. In order to permit repeat-pass interferometry applications like subsidence mapping or glacier monitoring, the cross-track distance between radar acquisitions in repeated orbits should be as small as possible. Depending on the availability of digital elevation models, which are used to compensate topographic effects, cross-track distances below 350 m are desirable. Hence, the TSX osculating orbit is controlled within a “tube” defined about an Earth-fixed reference trajectory over the entire mission lifetime. In order to fulfill the requirements, the radius of the “tube” is set to 250 m, which corresponds to the maximum allowed deviation of TSX from the reference orbit in the plane perpendicular to the flight direction in the rotating Earth-fixed system. This is very challenging, considering the low 505 km altitude with the highly dynamic disturbance forces acting on the satellite.

The TSX orbit control concept was firstly presented at the International Symposium on Space Flight Dynamics (ISSFD) in 2004 [2]. The experience gained during launch and early operations as well as the target orbit acquisition process were presented at the ISSFD in 2007 [3]. In the present work we complete the description of the orbit control strategy and present in-flight results gained within more than six years of operations. We show that both the implemented

reference orbit and the orbit control concept have proved to work remarkably well, and that the tight control requirement is fully met.

Table 1 summarizes the TSX reference orbit (REF) characteristics and the mean orbital elements, which are derived from the osculating elements by applying a modified Eckstein-Ustinov theory [4]. In contrast to traditional design considerations for Sun-synchronous, frozen eccentricity repeat orbits, the TSX reference orbit must be a closed orbit with matching states at the beginning and end of each 11-day repeat cycle. Therefore, the reference orbit design was formulated as an optimization problem [5]. The implemented TSX reference orbit is expressed in an Earth-fixed frame (ITRF2000) and forms the basis for both orbit control and mission planning including the scheduling of SAR acquisitions. It is repeated in 11-day intervals throughout the entire mission.

The TSX spacecraft is depicted in Figure 1. The characteristics which are relevant for our orbit control purposes are a launch mass of 1340 kg, a 10 m² cross-section for radiation pressure computation and 3.2 m² for drag. The spacecraft is equipped with both single- (MosaicGNSS) and dual-frequency (IGOR) GPS receivers, enabling precise on-ground orbit determination with cm-accuracy [6]. At launch, TSX carried 78 kg of hydrazine propellant and a redundant set of four 1-Newton thrusters.

Orbit type	Sun-synchronous repeat orbit
Repeat period	11 days
Repeat cycle	167 orbits in the repeat
Orbits per day	15 + 2/11
Local time of ascending node	18:00
Eccentricity, e	0.00125 (frozen)
Inclination, i	97.446°
Argument of perigee, ω	90.0°
Semi-major axis, a	6883.513 km

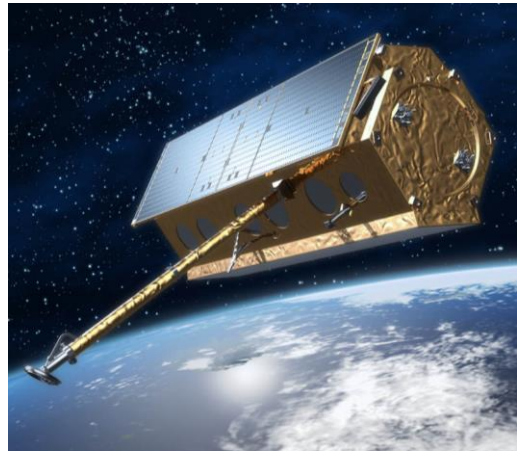


Figure 1. The TerraSAR-X spacecraft.

Table 1. TerraSAR-X reference orbit characteristics and mean orbital elements.

2. Space Error Parameterization

For the purpose of orbit monitoring and control we define a variable called space error E . Every orbital revolution is divided into 36 equally spaced check points k , at which the space error is evaluated in a pseudo orbital frame. As illustrated in Fig. 2, E is found from the vector difference between the position of the real orbit (TSX) and the reference orbit (REF) at the time where the along-track component of the position difference is zero. The Earth-fixed REF ephemeris is defined for the first 11 days of the mission (i.e. June 15-26, 2007) and repeats thereafter. Thus, before determining the space error, a time mapping has to be applied at any check point k , which relates the REF time t_k to the current time t_k^* by $t_k^* = t_k + z \cdot 11d + \Delta t$, with z being the integer number of 11-day repeat cycles completed since launch, and Δt being the time equivalent of the un-controlled TSX-REF along-track displacement.

Note that the frame for the space error evaluation is not derived from the inertial position and velocity vectors, but rather from the Earth-fixed vectors, which is why we use the term pseudo orbital frame. This convention has been implemented within both orbit and attitude control. For the latter, the so-called Total Zero Doppler Steering is applied, which aligns the SAR antenna azimuth axis with the ground-track by means of small yaw and even smaller pitch offsets between the satellite body frame and the orbital frame. The yaw offset is actually the angle enclosed by the Earth-fixed and inertial velocity vectors, which is up to 3.7° at equator crossings.

The orbit control requirement for TSX is to keep the space error $E \leq 250$ m at every point k in the osculating orbit. This corresponds to a toroidal tube with 250 m radius around the reference orbit. As illustrated in Fig. 2 the space error is a vector with components in the pseudo orbit radial and normal directions, E_R and E_N , respectively.

3. Space Error Evolution

TSX is flying in a frozen, sun-synchronous repeat orbit at 505 km altitude (cf. Tab. 1). The most important disturbance force acting on the satellite is the atmospheric drag. The decay of the semi-major axis changes the orbital period, which in combination with the Earth rotation causes a change in the ground-track. In the following, we will not present a complete analytical relation between orbital elements and space error components (for formal relationships refer to [7]). Nevertheless a basic understanding is necessary in order to study the orbit control strategy.

For simplicity we focus on the evolution of the space error at ascending node passes. The evolution at different points in orbit might then be derived taking into account the orbit inclination, actual latitude and TSX-REF inclination difference. The normal space error at the ascending node, $E_{N,0}$, is strictly related to the TSX-REF longitude difference at the ascending node, $\Delta\lambda_0$:

$$E_{N,0} = r \cdot \Delta\lambda_0 \cdot \sin(i + \alpha_0) \quad (1)$$

with r being the norm of the position vector, i being the inclination, and α_0 being the angle enclosed by the inertial and Earth-fixed velocity vectors at the ascending node, i.e. $\alpha_0 = 3.7^\circ$. By definition $\Delta\lambda$ is positive in westward direction.

For a near-circular orbit and considering only a second order geo-potential, the variation in the longitude difference may be deduced as [8]

$$\Delta\lambda_0 = \lambda_{TSX,0} - \lambda_{REF,0} = k_1(t - t_M) + 0.5 \cdot k_2(t - t_M)^2 \quad (2)$$

with

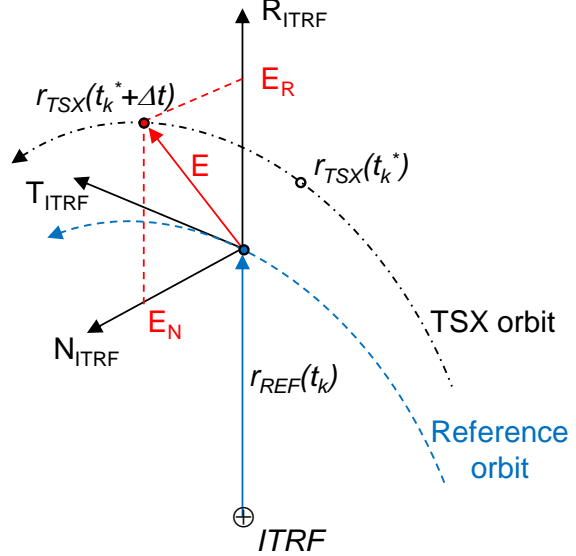


Figure 2. Space error definition: the space error is evaluated in the plane perpendicular to flight-direction at any REF check point k . In this example, TSX arrives at check point k later than REF (time increment Δt).

$$k_1 = \frac{1}{P_\Omega} \left(\frac{\partial \lambda_{TSX}}{\partial a} \Delta a_0 + \frac{\partial \lambda_{TSX}}{\partial i} \Delta i_0 \right) \quad \text{and} \quad k_2 = \frac{1}{P_\Omega} \left(\frac{\partial \lambda_{TSX}}{\partial a} \frac{da}{dt} + \frac{\partial \lambda_{TSX}}{\partial i} \frac{di}{dt} \right)$$

where $(t-t_M)$ is the time since the last control maneuver, a is the semi-major axis (SMA), and P_Ω is the nodal period. Approximations for the partial derivatives of the longitude drift with respect to a and i can be found in [8], [9]. In the following we disregard the inclination change di/dt , which is very small for our Sun-synchronous orbit, and assume the decrease in the semi-major axis da/dt to be constant, i.e.

$$\frac{da}{dt} = -\rho \cdot \frac{C_D A}{m} \sqrt{\mu \cdot a} \quad (3)$$

with ρ being the constant atmospheric density, $C_D A/m$ being the ballistic coefficient of the spacecraft, and $\mu = 398600.4415 \text{ km}^3/\text{s}^2$.

From substitution of (2) into (1) we find a parabolic time variation of the normal space error at the equator. To illustrate the problem we apply the orbit characteristics given in Tab. 1, a moderate decay rate of $da/dt = 15 \text{ m/d}$, an initial TSX-REF difference in the semi-major axis of $\Delta a_0 = 40 \text{ m}$ and an inclination difference of $\Delta i_0 = 0$. The resulting normal space error evolution is depicted in Fig. 3.

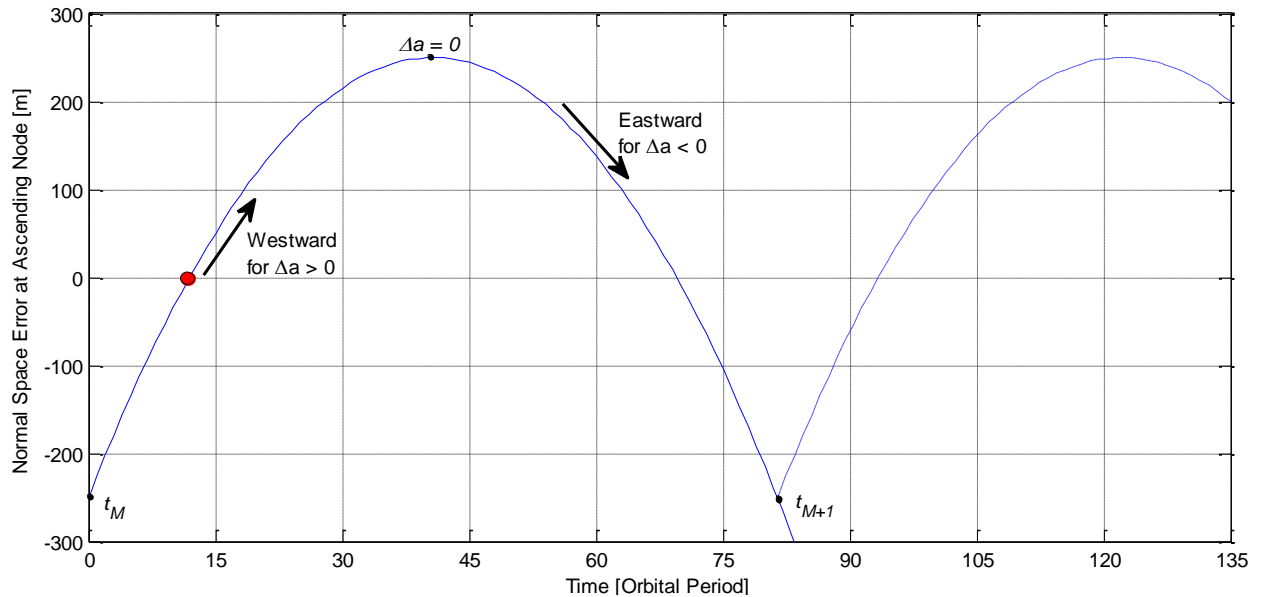


Figure 3. Ideal evolution of the normal space error at ascending nodes.

The starting point for our discussion of the space error evolution in Fig. 3 is indicated by a red dot at $t \approx 12$ orbital periods. Here, the TSX SMA is about 28 m higher than the REF SMA. Consequently, the nodal period of TSX is larger than for REF, and TSX arrives at the equator later than REF. Because of the Earth's eastward rotation, the TSX ground-track shifts towards the west of the REF ground-track. The larger the SMA offset, the stronger the ground-track drift. The drift of the normal space error is naturally reversed when the TSX-REF semi-major axis difference becomes negative. For our ideal scenario this happens in the middle of the maneuver cycle $[t_M, t_{M+1}]$ at $t \approx 41$ orbital periods. The eastward shift continues to grow as the SMA difference increases. At $t \approx 81$ orbital periods the lower limit of the normal space error is

reached, and SMA raising is necessary to revert the space error drift. In our example, the tangential maneuver takes place at t_{M+1} and raises the SMA by 80 m. Thereafter, the evolution repeats.

As discussed, the evolution of the normal component of the space error E_N is mainly affected by atmospheric drag. In addition, we have to consider the TSX-REF inclination difference Δi , which is subject to perturbations by the luni-solar potential and the solar radiation pressure. The inclination difference directly contributes to the normal space error, which at an arbitrary argument of latitude u (u is the sum of the argument of perigee ω and the mean anomaly M , i.e. $u = \omega + M$) can be modelled as

$$E_N = r \cdot \sin(i + \alpha) \cdot [\Delta \lambda \cos(u) + \Delta i \sin(u)]. \quad (4)$$

Besides the obvious impact of the inclination difference on E_N , Δi also causes a change in the Right Ascension of the Ascending Node (RAAN), which then contributes to the longitude drift and the normal space error (cf. partial derivatives in eq. (2)).

The corresponding radial space error ΔE_R depends on the TSX-REF differences in semi-major axis and eccentricity vector. The latter is mainly perturbed by the geo-potential and the solar radiation pressure. The radial space error can be modelled as

$$E_R = \Delta a + r \cdot \Delta e_x \cos(u) + r \cdot \Delta e_y \sin(u). \quad (5)$$

Figure 4 depicts the ideal space error evolution over one maneuver cycle. Again we consider an ideal scenario, where eccentricity vector differences are neglected and the radial space error corresponds to the semi-major axis difference. The control limit is indicated by a green circle with 250 m radius. In accordance with Fig. 3, the orbit raising maneuver Δv takes place at the eastern violation of the control tube.

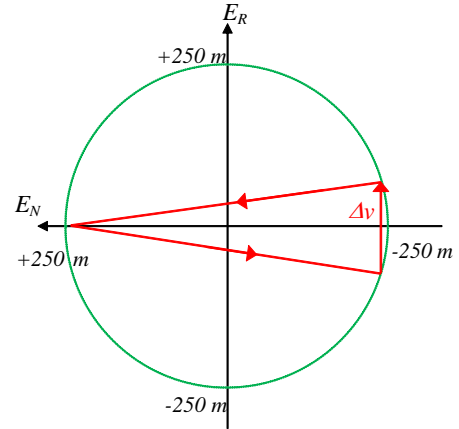


Figure 4. Ideal evolution of the TSX-REF space error at ascending nodes.

So far we only considered ideal scenarios. In reality the uncertainty in the predicted evolution of solar flux and geomagnetic index over the next maneuver cycle directly affects the density and hence atmospheric drag prediction. Thus, in practice we experience two non-ideal scenarios. Firstly, if the planned maneuver is larger than required, the decay takes too long and the tube is violated at the left side in Fig. 4, i.e. $E_N > +250$ m. Secondly, if the planned maneuver is smaller than required (i.e. from underestimating drag) the drift return starts too early, i.e. at $E_{N,max} < +250$ m. For an analysis of the impact of the orbit prediction accuracy on the space error prediction please refer to [11]. Furthermore, violations of the eastern boundary may result from operational conflicts, i.e. if the necessary orbit raising maneuver has to be postponed.

4. Control Concept

In the previous section we have analyzed the relation between the space error and the orbital elements. The necessary increments in the orbital elements can be translated into velocity increments Δv by applying the Gauss equations adapted to near-circular orbits [9]:

$$\begin{aligned}
\Delta a &\approx \frac{2a}{v} \Delta v_T \\
\Delta e_x &\approx \frac{2 \cos u}{v} \Delta v_T + \frac{\sin u}{v} \Delta v_R \\
\Delta e_y &\approx \frac{2 \sin u}{v} \Delta v_T - \frac{\cos u}{v} \Delta v_R \\
\Delta i &\approx \frac{\cos u}{v} \Delta v_N
\end{aligned} \tag{6}$$

where e_x and e_y are the eccentricity vector components built from the Keplerian elements e and ω , i.e. $(e_x, e_y)^T = e \cdot (\cos \omega, \sin \omega)^T$. It may be seen from these equations that the efficiency of a thrust in radial direction (Δv_R), performed to correct the eccentricity vector, is half that of a correction made in tangential direction (Δv_T). Therefore, only the latter is considered. Furthermore, from eq. (6) we find the in-plane and out-of-plane control to be decoupled, justifying the implementation of independent control strategies. Before focusing on these strategies, we firstly discuss an important constraint.

At launch, the TerraSAR-X satellite was equipped with 78 kg of Hydrazine propellant. Four 1-Newton thrusters (and a set of four redundant thrusters) are mounted at the back of the satellite which during nominal operations points in anti-flight direction. The slight canting of the thrusters enables the generation of attitude control torques during emergency attitude operations. The 1-Newton thrusters were qualified in the frame of the Globalstar program and have successfully been flown on various missions, e.g. Globalstar, Jason-1, Cosmo-Skymed, Radarsat-2, etc. [10].

In order to save cost, the thrusters were not re-qualified for the TerraSAR-X mission. Although the thrusters were qualified for 59,000 cycles (i.e. hot pulses), only about 1,400 qualification tests were performed for cold pulses with one hour of pre-heating. Every standard orbit control maneuver begins with one of these cold pulses (with pre-heating) followed by several hot pulses. Considering margins and the allocation to thruster activity during attitude safe mode etc. a total design budget of 578 pulses (or maneuvers) was allocated for orbit control purposes. This constraint drives the selection of a maneuver planning scheme based on single pulses, rather than pairs of maneuvers. Furthermore, we are trying to maximize the maneuver cycle.

4.1. In-plane Control

The radial contribution E_R of the space error results from changes in semi-major axis and eccentricity (cf. eq. 5). There are no specific maneuvers planned for controlling E_R , because of the limited amount of cold pulses with pre-heating. However, the radial space error is controlled by distributing the E_N in-plane control maneuvers over an optimized position within the orbit. Therefore the size of the in-plane maneuvers is driven by the E_N -control, whereas the location of the maneuvers is driven by the E_R -control.

In order to save thruster pulses and thereby minimize the instrument outage time, the time between consecutive in-plane maneuvers has to be maximized. The approach for this optimization is explained in the following. If the predicted space error exceeds the control requirements, a tangential maneuver with the necessary velocity increment Δv_T is calculated. The first guess on this Δv_T is given by solving the first Gauss equation (eq. 6). From the numerical orbit propagation the evolution of the predicted space error is found for the initial guess (dashed blue curve in Fig. 5). Within an iterative process a Newton search approach is applied to find the

optimal Δv_T . The target is to let the space error use the whole bandwidth of the control dead-band limits, i.e. [-250 m, +250 m]. Figure 5 depicts the evolution of the predicted normal space error E_N at ascending nodes for different steps within the iteration process (blue curves). In addition, E_N is shown at all latitudes for the final maneuver iteration (gray curve).

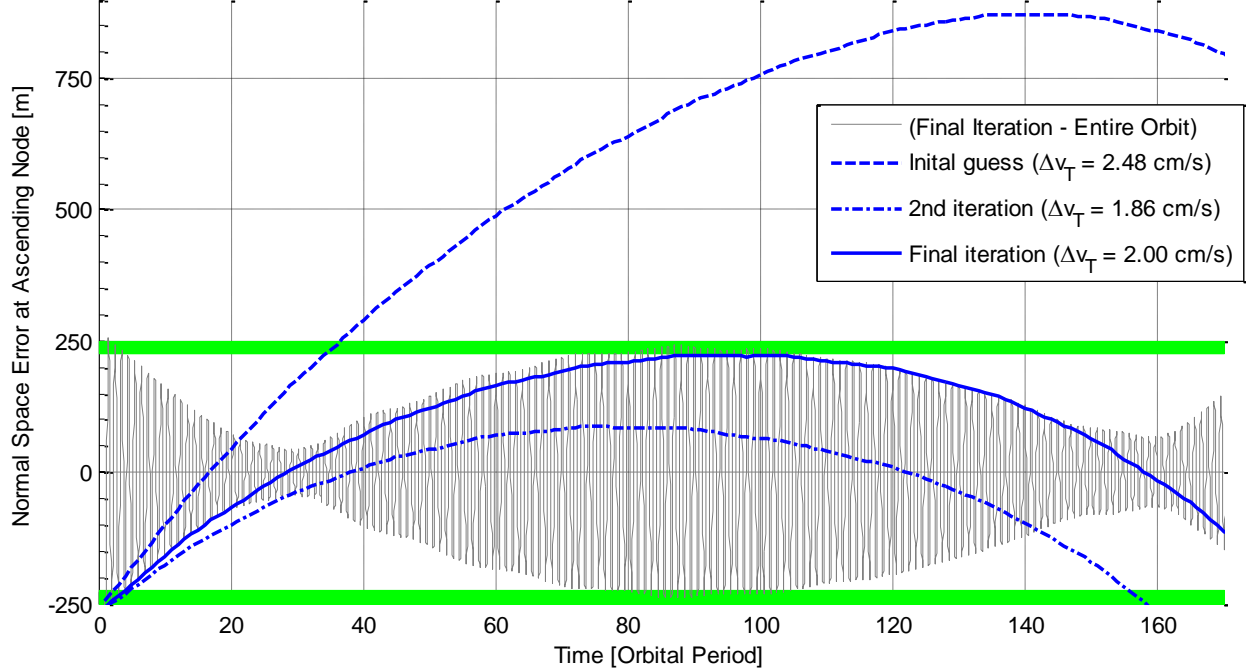


Figure 5. Predicted evolution of the normal space error at ascending nodes within the iterative maneuver planning process. The in-plane maneuver is planned for Feb. 6, 2011. The green bands are [-250 m, -225 m] and [+225 m, +250 m]. The normal space error at all latitudes is given for the final iteration only (gray).

So far, we know the size of the in-plane maneuver and the approximate maneuver epoch, which follows from the epoch of dead-band violation within the previous maneuver cycle and constraints related to mission planning. The exact maneuver epoch is then determined from the best maneuver location in an active eccentricity control sense.

From eq. (6) we find the optimized Δv_T to be sufficient to change the TSX eccentricity vector by

$$\Delta e = \sqrt{\Delta e_x^2 + \Delta e_y^2} = \frac{2}{v} \Delta v_T. \quad (7)$$

In general, the required variation in the eccentricity vector $\Delta e_{req} = |\vec{e}_{TSX} - \vec{e}_{REF}|$ does not equal Δe generated by the tangential maneuver Δv_T . The problem could be solved exactly by distributing the orbit raising maneuver over two maneuvers Δv_{T1} and Δv_{T2} with $\Delta v_T = \Delta v_{T1} + \Delta v_{T2}$. Then, if the required eccentricity change exceeds the necessary SMA change, i.e. $a \cdot \Delta e_{req} > \Delta a_{req}$, additional fuel would be spent to control the eccentricity vector precisely, i.e. $\Delta v_T < |\Delta v_{T1}| + |\Delta v_{T2}|$.

As already stated the maneuver pulse budget does not allow such an expensive approach, thus only a single maneuver is used and optimized in order to achieve a frozen orbit as close as possible to the reference orbit. The active eccentricity control idea is depicted in Figure 6, which

shows the evolution of the TSX-REF relative eccentricity vector over a two-day period with the in-plane maneuver from Fig. 5 in the middle. The argument of latitude of the maneuver is chosen in order to minimize the TSX-REF eccentricity vector difference after the maneuver Δv_T . Clearly, the maneuver induced change of the relative eccentricity vector points towards the eccentricity vector of the reference orbit (0, 0).

4.2. Out-of-plane Control

Changes in the TSX-REF relative inclination, which are mainly caused by sun and moon third body perturbations, contribute to the normal space error at non-zero latitudes. The largest impact is at the poles where the inclination-induced normal space error is almost $a \cdot \Delta i$ (cf. eq. 4). The un-controlled TSX orbit would vary over 0.005° in total per year, which is equivalent to a 600 m normal space error at polar crossings, which clearly would exceed the control limits. Therefore, the TSX-REF inclination deviation Δi is kept within $\pm 0.0015^\circ$ corresponding to a normal space error of 180 m at polar crossings.

Figure 7 depicts the out-of-plane maneuver planning process. The natural evolution of the TSX-REF relative inclination is illustrated in red. An inclination correction maneuver is triggered when the predicted relative inclination violates the control limit. The maneuver size is optimized in order to maximize the out-of-plane maneuver cycle.

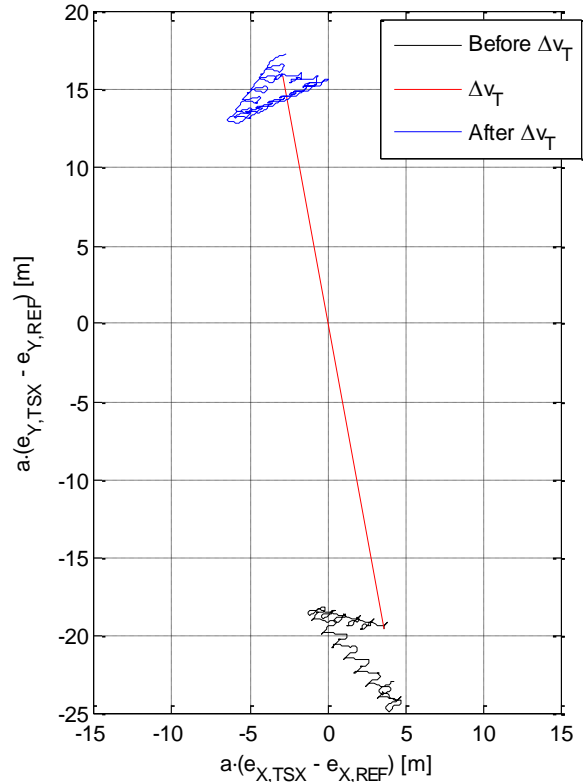


Figure 6. Active eccentricity control concept: Natural evolution of the TSX-REF relative eccentricity vector within a 2-day period with a maneuver ($\Delta v_T = 2$ cm/s) in the middle. The perturbations by geo-potential and solar radiation pressure onto the relative eccentricity vector are small as compared to the maneuver impact.

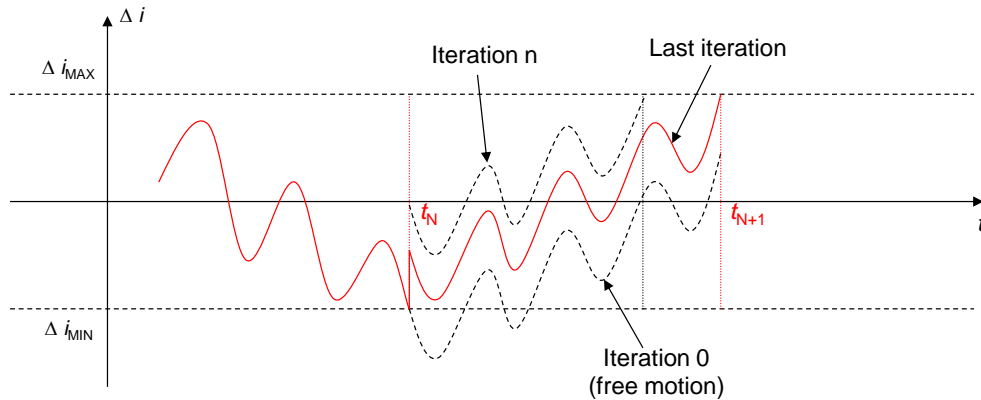


Figure 7. Out-of-plane maneuver planning process.

In general, the normal space error E_N could be controlled by increments in the RAAN, too. In practice however, only the semi-major axis is corrected as this is more economical in terms of Δv and instrument outage time because an out-of-plane maneuver requires a time-consuming 90° yaw slew. Thus, the out-of-plane control solely comprises inclination correction, while the TSX-REF RAAN difference is un-controlled.

5. Flight Results

Within more than six years of TerraSAR-X operations almost 500 orbit control maneuvers have been performed. With increasing solar activity we experienced strong variations in solar flux and geomagnetic activity, which significantly affected the air density and hence the orbit decay.

Figure 8 (top) depicts the F10.7 cm solar flux evolution, which serves as an indicator for the solar activity, over the years 2009 to 2013. The diagram below summarizes all in-plane maneuvers performed in the same period. Obviously, during low solar activity in year 2009 the maneuvers were relatively small ($\Delta v_T \leq 1$ cm/s) and the typical period between two successive maneuvers was 10 to 14 days. In contrast, maneuvers with sizes of up to 5 cm/s and maneuver cycles of 2 to 3 days only were necessary to precisely control the TSX orbit during periods of high solar activity, e.g. at end of 2012 and beginning of 2014. The out-of-plane control is independent of the solar activity. On average, 3 to 5 out-of-plane maneuvers have been performed per year, with maneuver sizes between 10 and 30 cm/s.

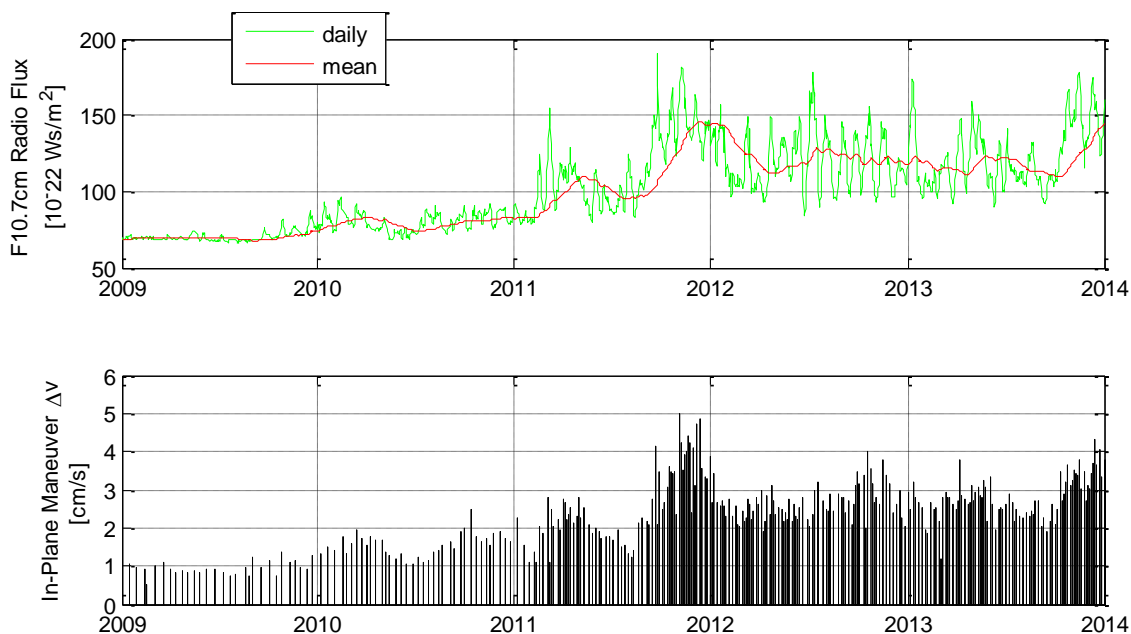


Figure 8. F10.7 cm Solar Flux (top) and TSX in-plane maneuver activity in period 2009-2013.

The achieved TSX orbit control performance is summarized in Tab. 2 for the year 2009 and the first quarter of year 2014, i.e. for periods of low and high solar activity, respectively. Clearly, the control accuracy requirement of $E \leq 250$ m has fully been met in a root mean square (RMS) sense. Furthermore, more than 99 % of all check points are inside the 250 m control tube.

As an example, the space error evolution is depicted in Fig. 9 for the last quarter of 2009. The plot comprises 1,397 orbits in total, which almost entirely are within the 250 m control tube (red circle). There is one interesting orbit that violates the tube in radial direction. This event is related to a debris collision avoidance maneuver. On Nov. 27, 2009 a maneuver with $\Delta v_T = 7.7$ cm/s was executed to raise the SMA by 130 m and thereby increase the radial separation to a Cosmos 2251 debris by 260 m. The maneuver was executed half an orbital period before the time of closest approach, and a corresponding maneuver to lower the SMA was carried out one revolution later.

R.M.S.	2009	2014, 1 st qu.
E_R [m]	19.5	35.0
E_N [m]	107.5	102.2
E (2D) [m]	109.3	108.0

Table 2. TSX Orbit Control Performance in 2009 and 1st quarter of 2014.

Besides the single event in Fig. 9, we find the space error to be dominated by the normal component E_N . This is related to the small orbit control maneuvers (typically 1 cm/s, cf. Fig. 8) performed in 2009 during the solar minimum. The corresponding change in the TSX-REF relative eccentricity vector was below 20 m. A different behavior is found for periods of increased solar activity, e.g. during the first quarter of year 2014. Figure 10 depicts the evolution of the space error (left) and the relative eccentricity vector (right) during this period. Clearly, the larger maneuvers (up to 5 cm/s) have a stronger impact onto the radial space error, which is now confined within $-100 \text{ m} < E_R < 100 \text{ m}$ as compared to the year 2009 with $-30 \text{ m} < E_R < 30 \text{ m}$. The diagram in Fig. 10 (right) proves the chosen concept of active eccentricity vector control by a single in-plane maneuver.

In summary, both the implemented reference orbit and the orbit control concept have proved to work remarkably well. The tight control requirement is fully met even enabling the scientific and commercial users to determine the heights and to detect millimeter-scale structural deformations of large buildings from repeat-pass interferometry [12]. Other interferometric applications that have been made possible by the precise TSX orbit control are, for example, the detection of small movements of the Earth's surface caused by tectonics, volcanism, earthquakes, and landslides. The precise orbit control and the outstanding orbit determination accuracy make TerraSAR-X to an imaging instrument with geodetic qualities [13].

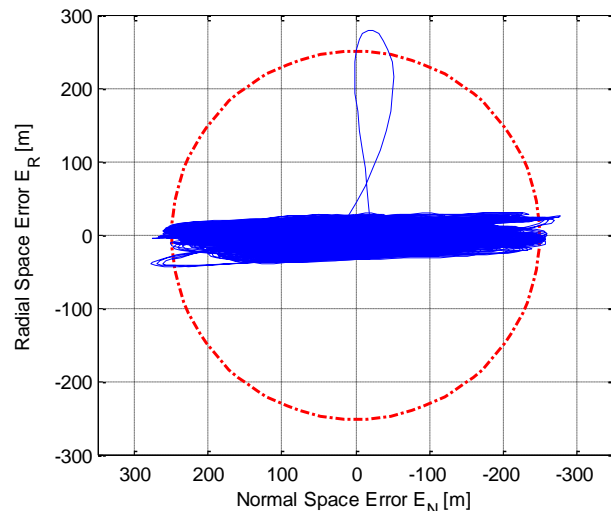


Figure 9. TSX orbit control performance during the last quarter of year 2009. The dashed red line indicates the 250 m orbit control tube. The single orbit violating the upper radial limit resulted from a debris collision avoidance maneuver on 2009/11/27.

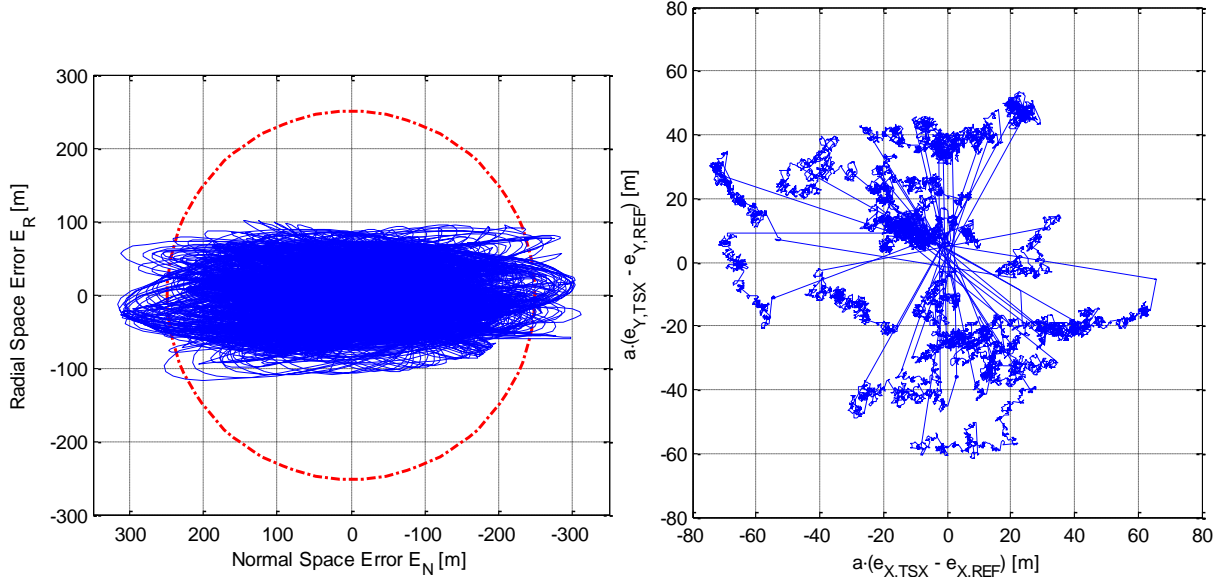


Figure 10. TSX orbit control performance (left) and TSX-REF relative eccentricity vector during the first quarter of year 2014.

6. Conclusions

The TSX osculating orbit is controlled within a “tube” of 250 m radius defined about an Earth-fixed reference trajectory over the entire mission lifetime. For orbit monitoring and control, the variable space error E has been introduced, which is evaluated in the radial and normal directions within a pseudo orbital frame. The evolution of the space error in the 505 km altitude orbit has been analyzed and control strategies for the decoupled in-plane and out-of-plane orbit control have been derived. The implemented out-of-plane control concept maintains the TSX-REF inclination difference within $\pm 0.0015^\circ$, while the RAAN difference is un-controlled. A single-maneuver concept has been developed for the in-plane control, which maximizes the time between consecutive maneuvers. The size of the in-plane maneuvers is driven by the predicted evolution of the normal space error, whereas the location of the maneuvers is chosen in order to actively control the eccentricity vector.

Flight results gained within more than six years of operations have been presented. During low solar activity the in-plane maneuvers were relatively small ($\Delta v_T \leq 1$ cm/s) and the typical period between two successive maneuvers was 10 to 14 days. In contrast, maneuvers with sizes of up to 5 cm/s and maneuver cycles of 2 to 3 days only were necessary to precisely control the TSX orbit during periods of high solar activity. The out-of-plane control is independent of solar activity, and on average, 3 to 5 out-of-plane maneuvers are performed per year, with maneuver sizes between 10 and 30 cm/s.

The implemented reference orbit and the orbit control concept have proved to work remarkably well, and the tight orbit control requirement of $E \leq 250$ m has fully been met in a root mean square (RMS) sense. Furthermore, more than 99 % of the time TSX was inside the 250 m control tube. The precise orbit determination and control make TerraSAR-X to an imaging instrument with geodetic qualities. For example, millimeter-scale structural deformations of large buildings can be detected from TerraSAR-X repeat-pass interferometry.

7. References

- [1] Werninghaus, R., Buckreuss, S., “The TerraSAR-X mission and system design”, *IEEE Trans. Geosci. Remote Sens.*, 48, pp. 606–614 (2010).
- [2] Arbinger, C., D'Amico, S., Eineder, M., “Precise Ground-In-the-Loop Orbit Control for Low Earth Observation Satellites”, *18th International Symposium on Space Flight Dynamics*, Munich, Germany (2004).
- [3] Kahle, R., Kazeminejad, B., Kirschner, M., Yoon, Y., Kiehling, R., D'Amico, S., “First In-orbit Experience of TerraSAR-X Flight Dynamics Operations”, *20th International Symposium on Space Flight Dynamics*, Annapolis, USA (2007).
- [4] Spiridonova, S., Kirschner, M., Hugentobler, U., “Precise Determination of Mean Orbital Elements for LEO Monitoring and Maintenance”, *24th International Symposium on Space Flight Dynamics*, Laurel, MD, USA (2014).
- [5] D'Amico, S., Arbinger Ch., Kirschner M., Campagnola S., “Generation of an Optimum Target Trajectory for the TerraSAR-X Repeat Observation Satellite”, *18th International Symposium on Space Flight Dynamics*, Munich, Germany (2004).
- [6] Wermuth, M., Hauschild, A., Montenbruck, O., Jäggi, A., “TerraSAR-X Rapid and Precise Orbit Determination”, *21st International Symposium on Space Flight Dynamics*, Toulouse, France (2009).
- [7] De Florio, S., D'Amico, S., Radice, G., "Virtual Formation Method for Precise Autonomous Absolute Orbit Control", *Journal of Guidance, Control, and Dynamics*, 37 (2), pp. 425-438 (2014).
- [8] Vallado, D.A., “Fundamentals of Astrodynamics and Applications”, ISBN 1-881883-12-4 (2001).
- [9] Micheau, P., “Orbit Control Techniques for Low-Earth Orbiting (LEO) Satellites”, in Carrou, J-P. (Editor), *Spaceflight Dynamics*, CNES (1995).
- [10] Airbus Defence & Space, “1 N Hydrazine Thruster”, <http://cs.astrium.eads.net/sp/spacecraft-propulsion/hydrazine-thrusters/1n-thruster.html> (2014).
- [11] Arbinger, C., D'Amico, S., “Impact of Orbit Prediction Accuracy on Low Earth Remote Sensing Flight Dynamics Operations”, *18th International Symposium on Space Flight Dynamics*, Munich, Germany (2004).
- [12] Eineder, M., Adam, N., Bamler, R., Yague-Martinez, N., Breit, H., “Spaceborne Spotlight SAR Interferometry with TerraSAR-X”, *IEEE Transactions on Geoscience and Remote Sensing*, 47 (5), pp. 1524-1535 (2009).
- [13] Eineder, M., Minet, C., Steigenberger, P., Cong, X., Fritz, T., “Imaging Geodesy - Toward Centimeter-Level Ranging Accuracy with TerraSAR-X”, *IEEE Transactions on Geoscience and Remote Sensing*, 49 (2), pp. 661-671 (2011).